2016

# Numerical simulation and experimental validation of a large-area capacitive strain sensor for fatigue crack monitoring

Xiangxiong Kong
*University of Kansas*

Jian Li
*University of Kansas*

Caroline Bennett
*University of Kansas*

***See next page for additional authors***

# Numerical simulation and experimental validation of a large area capacitive strain sensor for fatigue crack monitoring

Xiangxiong Kong [a], Jian Li [a*], Caroline Bennett [a], William Collins [a], and Simon Laflamme [b,c]

[a]Department of Civil, Environmental and Architectural Engineering,
University of Kansas, Lawrence, KS 66045, USA
[b]Department of Civil, Construction, and Environmental Engineering,
Iowa State University, Ames, IA, 50011, USA
[c]Department of Electrical and Computer Engineering,
Iowa State University, Ames, IA, 50011, USA

## Abstract

A large area electronics in the form of a soft elastomeric capacitor (SEC) has shown great promise as a strain sensor for fatigue crack monitoring in steel structures. The SEC sensors are inexpensive, easy to fabricate, highly stretchable, and mechanically robust. It is a highly scalable technology, capable of monitoring deformations on mesoscale systems. Preliminary experiments verified the SEC sensor's capability in detecting, localizing, and monitoring crack growth in a compact tension specimen. Here, a numerical simulation method is proposed to simulate accurately the sensor's performance under fatigue cracks. Such method would provide a direct link between the SEC's signal and a fatigue crack geometry, extending the SEC's capability to dense network applications on mesoscale structural components. The proposed numerical procedure consists of two parts: 1) a finite element analysis for the target structure to simulate crack growth based on an element deletion method; 2) an algorithm to compute the sensor's capacitance response using the FE analysis results. The proposed simulation method is validated based on test data from a compact tension specimen. Results from the numerical simulation shows good agreement with SEC's response from the laboratory tests as a function of the crack size. Using these findings, a parametric study is performed to investigate how the SEC would perform under different geometries. Results from the parametric study can be used to optimize the design of a dense sensor network of SECs for fatigue crack detection and localization.

*Keywords*: fatigue crack monitoring, sensing skin; structural health monitoring; compact tension specimen; finite element model; capacitive strain sensor, large area electronics, dense sensor network, soft elastomeric capacitor.

[*]Assistant Professor; Email: jianli@ku.edu

## 1. Introduction

Fatigue cracks caused by fluctuating stresses and strains are one of the major mechanisms of damage to structural components. Stress concentration due to small defects in material leads to accumulation and nucleation of the defects, which ultimately result in fatigue cracks. In civil engineering, fatigue cracks in steel bridges are a great concern for local governments, motorists, and pedestrians. Fatigue cracks in their initial phase are usually small in size and hence difficult to detect. Moreover, depending on loading conditions and structural layouts, these cracks may develop rapidly and weaken structural integrity[1,2].

Monitoring fatigue cracks is essential so that appropriate retrofits can be applied before they reach critical size. To date, visual inspection has been the most common method for fatigue crack detection in steel bridges for its simplicity. However, this method is also labor intensive, costly, and prone to error. Although nondestructive evaluation (NDE) techniques, such as dye penetration, eddy current, magnetic particles, and ultrasonic testing, can be applied to improve the accuracy of crack detection during bridge inspection, the need for extensive human involvement makes them unsuitable for autonomous and continuous monitoring of fatigue cracks. Acoustic emission and piezoelectric sensor based techniques [3, 4] have received great attention in crack detection. However, both methods require complex algorithms for data processing and the results may be sensitive to noise. Computer vision-based crack identifications techniques have been applied to steel girder [5] and concrete bridges[6]. Relying on imaging processing, this approach mimics traditional human inspection to identify cracks. However, processing a large volume of images can be time consuming, and the robustness of results can be sensitive to the feature of specific types of cracks. A comprehensive review of crack detection methods can be found in Yao et al. [7]

Direct strain measurement has the potential to be very effective for crack detection since crack opening leads to abrupt strain change in the localized area. For this reason, both traditional metal foil gages [8] and fiber optic sensors [9] have been evaluated for crack detection. One general agreement is that cracks can be effectively detected using direct strain measurement if they are in direct contact with or close proximity to the sensor. Since the location of fatigue cracks are not known as a priori, to effectively detect cracks, a large number of foil gages would be needed. Fiber optic sensors are able to monitor strain over a long distance, but may still be limited considering cracks can occur randomly over a large two-dimensional surface. In addition, the limited ductility of the sensing materials leads to breakage of the sensors under cracking, which prevents monitoring of further crack activities.

Recently, novel strain sensors which measure strains over a large area have shown their potential in crack detection. These sensors, often referred to as sensing skins, share one common feature of large size but operate under a wide variety of principles. Examples include carbon nanotube based sensors [10, 11], resistive sensor sheets [12], printable conductive polymer [13], patch antenna sensors [14, 15], and soft elastomeric capacitive (SEC) sensors [16, 17,18], etc. In particular, the SEC sensor is a highly scalable sensor due to its ease of fabrication and low cost materials. It is also highly stretchable, enabling a wide strain measurement range; the linearity of the SEC signal has been demonstrated for up to 20% strain [18].The SEC technology has been engineered to be deployed in sensing skin-type configurations. Analogous to biological skin, it would be able to measure local strain over a mesoscale area. Such configuration would enable fatigue crack detection, localization, and quantification.

Prior results on the characterization of the SEC have demonstrated its capacity to monitor static [17] and dynamic [19] strain in aluminum, steel, and concrete components. The authors have reported on the capability of the SEC to detect fatigue crack on small scale steel compact tension (CT) specimens, and also to localize such cracks leveraging a network configuration[20, 21, 22].

To enable large-scale deployment onto mesoscale systems for monitoring of fatigue cracks, it is critical to develop numerical models capable of linking the sensor's signal to a fatigue crack geometry. This would directly map a sensor network's response to a damage quantification, which information could easily be interpreted by infrastructure operators and managers to conduct condition-based maintenance procedures. Such numerical models could also be used in the design of a dense sensor network of SECs or similar skin-type sensors for the selection and placement of different sensor geometries throughout the network. In this paper, a numerical method based on finite element (FE) analysis is developed to simulate the SEC's capacitance response under fatigue cracks. An element removal technique in conjunction with a damage evolution model is adopted to simulate fatigue crack propagation in structural components. The SEC sensor is not explicitly included in the FE model. Instead, the FE model of the structural component is meshed in a way such that the deformation of the SEC sensor can be obtained directly from the FE model. A numerical algorithm is proposed to convert the deformation into capacitance response of the SEC sensor. The proposed numerical method is then validated based on experimental data from a CT specimen. Finally, a parametric study is performed to investigate the effect of changing the size of SEC sensor on its ability to detect fatigue cracks. The main contribution of this paper is the efficient and reliable numerical method for investigating the SEC sensor's performance under fatigue cracks generated under different structural configurations, boundary conditions, and loading conditions. The proposed method extends to other measurement devices of similar sensing principle.

## 2. Soft Elastomeric Capacitor (SEC) Sensor

This section provides a brief background on the SEC technology. Its sensing principle is first described, followed by the presentation of a typical results on its fatigue crack sensing capability. These results will later be used in the development of the numerical model.

### 2.1 Sensing principle

The SEC sensor is a flexible capacitor transducing a material elongation into a measurement change in capacitance. A detailed description on the sensor's fabrication procedure can be found in Laflamme et al. (2013) [16]. Briefly, its dielectric is composed of a styrene-ethylene/butylene-styrene (SEBS) block co-polymer filled with titania, and is sandwiched between two conductive plates fabricated from SEBS filled with carbon black (Figure 1). The SEC sensor can be fabricated with different sizes. In this study, the sensor dimension is 76 mm by 76 mm, with the effective sensing area 63.5 mm by 63.5 mm. Figure 1(c) is a picture of the SEC sensor used in this study, in which two copper tapes are embedded in the top and bottom electrodes (conductive plates) for connecting to the data acquisition system.

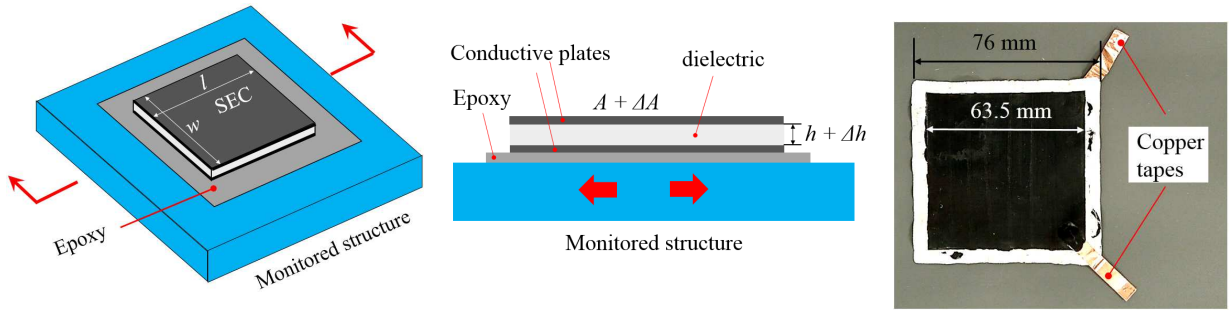


(a) (b) (c)

Figure 1. (a) Schematic of the SEC sensor; (b) SEC sensor under a tensile strain; and (c) a picture of the SEC sensor

The SEC can be attached to a structural surface using bonding agents such as epoxy. As illustrated in Figure 1(b), when the structures deforms, the surface strain provokes a change in the SEC's geometry by altering its area $A$ and thickness $h$. This change in geometry yields a change in the sensor's capacitance $C$

$$C = \frac{e_0 e_r A}{h} \tag{1}$$

where $e_0$ is the permittivity of air, $e_r$ is the permittivity of the dielectric, $A = w \cdot l$ is the sensing area of width $w$ and length $l$, and $h$ is the thickness of the dielectric.

## 2.2 Experimental validation for crack detection

The SEC sensor has been verified for fatigue crack detection through experimental tests of CT specimens [20, 21, 22]. The CT specimens were made by A36 steel with a thickness of 6.35 mm. The dimensions of the specimen are shown in Figure 2(a). To generate a fatigue crack, the specimen was connected to a pair of clevises which were mounted to a uniaxial load frame (Figure 2b). One SEC sensor was attached to one side of the specimen by epoxy, as shown in Figure 2(c). A commercial off-the-shelf data acquisition board (ACAM Pcap02) was connected to the top and bottom plates of the sensor to measure capacitance change of the sensor. A 2 Hz cyclic load with a constant load range from 0.65 kip (2.89 kN) to 6.5 kip (28.9 kN) was applied to the specimen. Capacitance measurements were sampled at 25 Hz.

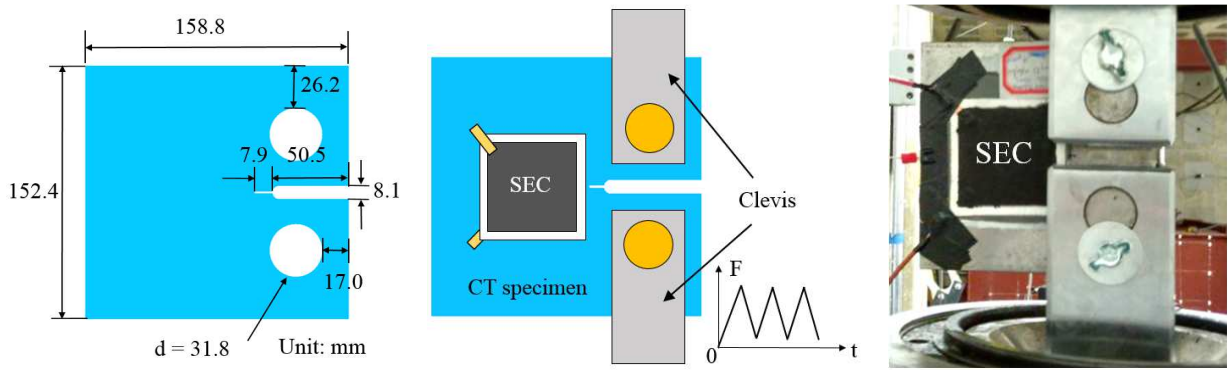


(a) (b) (c)

Figure 2. (a) Dimensions of the CT specimen; (b) schematic of test setup; and (c) picture of the test setup

Figure 3(a) shows a crack generated during the test. Figure 3(b) shows the sensor's response in terms of the peak-to-peak percentage change of capacitance (*PP C/C₀*), corresponding to different crack lengths with 1.59 mm (1/16 in.) increments. The crack length is taken as the distance measured between the tip of the crack and the edge of the sensing area, as illustrated in Figure 4. This distance reflects the length of the crack covered by the sensing area, which is about 7.9 mm away from the notch of the specimen. The peak-to-peak amplitude is selected because it provides a more robust measure of capacitance change over long-term monitoring, since the absolute capacitance of the SEC sensor may be subject to drift due to humidity and temperature changes. The result indicates that the SEC sensor is capable of detecting crack growth by showing an increasing change in *PP C/C₀* with increasing crack length.

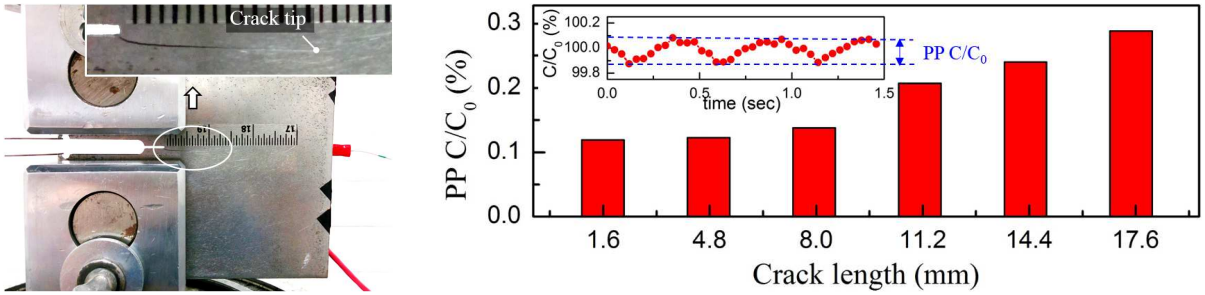


(a) (b)

Figure 3. (a) Crack growth in the CT specimen; and (b) percentage change of capacitance versus crack length

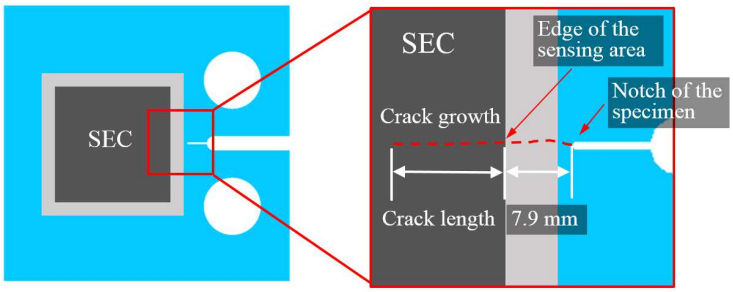


Figure 4. Illustration of crack length definition

## 3. Methodology for Numerical Simulation

This section presents the methodology used for the numerical simulations. First, the numerical approach is described. It is followed by a description of the procedure used in simulating crack growth. Lastly, the model of the SEC's electrical response is derived.

### 3.1 Numerical Approach

Figure 5 illustrates the overall procedure of the proposed numerical method using a CT specimen as an example. A four-step procedure is established: 1) identify crack-prone region of the structural member to determine the location for the SEC sensor; 2) create an FE model of the structural member to simulate the crack growth based on the element deletion method discussed in Section 3.2; 3) collect deformation results from the analysis of all elements within the location of the sensor; 4) compute the capacitance response of the SEC using the algorithm derived in Section 3.3. With

this procedure, the SEC sensor is assumed to be perfectly bonded to the structure, and its deformation taken as identical to the deformation of the structural member. The proposed numerical method is not limited to small scale CT specimens. It can be implemented on more complex structures of different scales, geometric configurations, and boundary conditions.

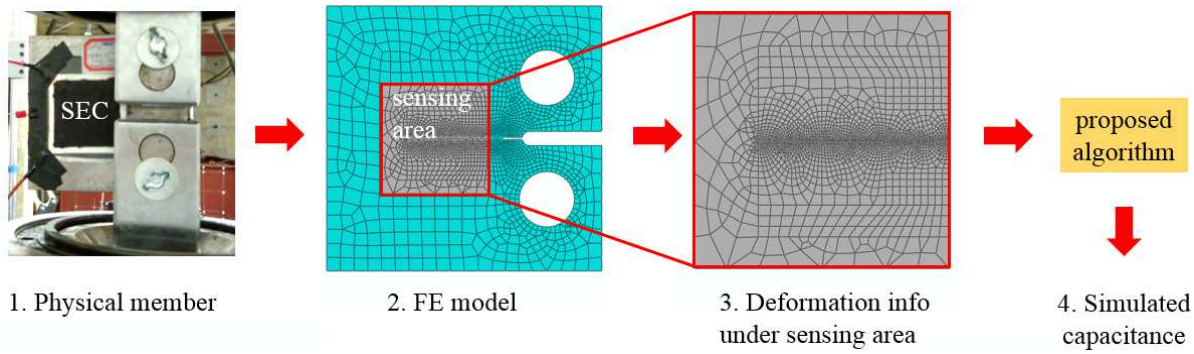


Figure 5. Procedure of the numerical approach

### 3.2 Crack growth simulation

In this study, finite element software package Abaqus 6.13 [23] is selected to simulate crack growth. In particular, the element deletion method is adopted to generate cracks in the model, which requires a damage evolution law defined in the material property so that the elements can accumulate damage and be removed from the model once they reach failure point. Several case studies in the literature indicate that the element deletion method can be applied in various applications such as the prediction of crack growth in structural components [24, 25], simulation of metal cutting process [26] and progressive collapse of building structures [27, 28], and so on.

The principle of the element deletion method is illustrated in Figure 6. The material is initially defined as a bilinear model. Then, a damage evolution mechanism is added to the model by defining an initial damage point and a failure point. Under such a damage mechanism, the element starts to accumulate damage once it passes the initial damage point, and it becomes completed damaged after reaching the failure point. The failure elements at the failure point are then removed automatically. By continually removing damaged elements, crack propagation can be numerically simulated, as shown in Figure 6(b).

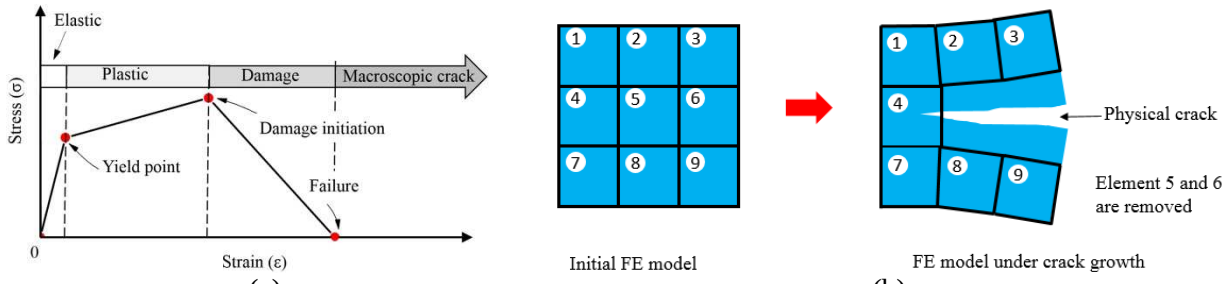


(a) (b)

Figure 6. Crack simulation through the element deletion method: (a) damage evolution model; and (b) simulation of crack growth by deleting elements where each numbered square is an element

### 3.3 Proposed algorithm for capacitance calculation

An algorithm is required to convert FE analysis results into sensor's response. Eq. (1) is the sensing principle of the SEC sensor, by which the capacitance can be computed once the sensing area $A$ and sensor's thickness $h$ are known. However, because the SEC sensor is not physically modeled, this equation cannot be applied directly since $h$ is not available. Eq. (2) [18] and Eq. (3) [20] describe the relationships between capacitance change and strain change for uniaxial and biaxial strain fields, respectively, where $C_0$ is the initial capacitance, $\varepsilon_x$ and $\varepsilon_y$ are the two principle strains, $v$ is the Poisson's ratio of the sensing material with a typical value of 0.49.

$$\frac{\Delta C}{C_0} = 2\varepsilon \tag{2}$$

$$\frac{\Delta C}{C_0} = \frac{1}{1-v}\left(\varepsilon_x + \varepsilon_y\right) \tag{3}$$

However, both equations are still difficult to be implemented in the FE analysis, because the strain result in FE analysis is commonly reported as the average strain of the element, while the true strain is difficult to obtain. Furthermore, the strain level highly relies on the mesh distribution, which may affect the accuracy of computation results. To overcome these challenges, a modified equation is proposed as follows.

The proposed equation for capacitance calculation directly builds a relationship between sensor's capacitance response and change of the sensing area. From Eq. (1), the capacitance change of the SEC sensor under deformation can be expressed as:

$$\frac{\Delta C}{C_0} = \frac{C_1 - C_0}{C_0} = \frac{e_0 e_r \left(\frac{A_1}{h_1} - \frac{A_0}{h_0}\right)}{e_0 e_r \frac{A_0}{h_0}} = \frac{A_1 h_0}{A_0 h_1} - 1 \tag{4}$$

where $C_0$, $A_0$, $h_0$ are the initial capacitance, sensing area, and thickness of the SEC sensor, respectively. $C_1$, $A_1$, $h_1$ are the corresponding values after the sensing skin deforms. By assuming incompressible sensing material ($A_0 h_0 = A_1 h_1$)[18], the thickness terms can be eliminated based on constant volume:

$$h_0 = \frac{A_1 h_1}{A_0} \tag{5}$$

Substituting Eq. (5) into Eq. (4), the capacitance change of the sensing skin becomes:

$$\frac{\Delta C}{C_0} = \frac{A_1^2}{A_0^2} - 1 \tag{6}$$

Eq. (6) is under the assumption that the sensor deforms uniformly within the area $A$. In practice, however, the SEC sensor is likely to experience highly nonuniform deformation or strain under fatigue cracks. To accommodate nonuniform deformation, the sensing area is discretized using finite element meshes. Assuming each element of the sensing area experiences uniform

deformation, Eq. (6) can be applied to each individual element. Within the sensing area *A*, the capacitance change of the i[th] element can be expressed as:

$$\frac{\Delta C_i}{C_{0i}} = \left(\frac{A_{1i}^{\ 2}}{A_{0i}^{\ 2}} - 1\right) \tag{7}$$

The initial capacitance for each individual element $C_{0i}$ is proportional to the area of the element $A_{0i}$:

$$C_{0i} = \frac{A_{0i}}{A_0} C_0 \tag{8}$$

Substituting Eq. (8) into Eq. (7), the capacitance change of the $i^{th}$ element becomes:

$$\Delta C_i = \frac{A_{0i}}{A_0} C_0 \left(\frac{A_{1i}^{\ 2}}{A_{0i}^{\ 2}} - 1\right) \tag{9}$$

The total capacitance change $\Delta C$ of the sensing area *A* is the summation of the capacitance change from all *n* elements, which can be expressed as:

$$\Delta C = \sum_{i=1}^{n} \Delta C_i = \frac{C_0}{A_0} \sum_{i=1}^{n} A_{0i} \left(\frac{A_{1i}^{\ 2}}{A_{0i}^{\ 2}} - 1\right) \tag{10}$$

Finally, the relative capacitance change becomes:

$$\frac{\Delta C}{C_0} = \frac{1}{A_0} \sum_{i=1}^{n} A_{0i} \left(\frac{A_{1i}^{\ 2}}{A_{0i}^{\ 2}} - 1\right) \tag{11}$$

The advantage of Eq. (11) is two-fold. First, it requires knowledge of only the areas of each element before and after deformation, which can be obtained directly from displacements of the nodes from the FE model. Second, a physical FE model of the SEC sensor is not required because the thickness of the sensor *h* is eliminated in the equation.

Based on Eq. (11), the proposed procedure for capacitance simulation can be established based on FE results. As illustrated in Figure 6, the initial area $A_{0i}$ and deformed area $A_{1i}$ of each individual element can be collected from the FE model, which are then substituted into Eq. (11) to compute capacitance change. Additionally, since the SEC sensor remains uncracked even though the underneath substrate has cracked, the area change of all deleted elements during crack propagation (i.e. element 5 and 6 as illustrated in Figure 7) are included in the computation. This is done to take into account sensor's measurement over the crack path even though they are physically removed from the model for crack simulation.

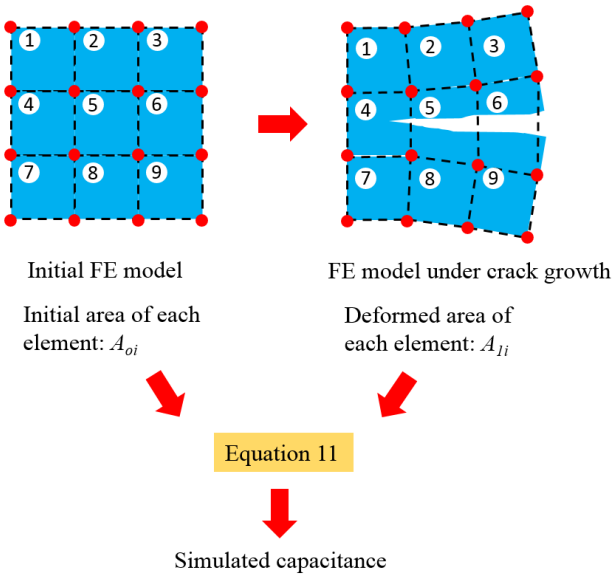


Figure 7. Propose procedure for simulating capacitance response of the SEC sensor based on FE analysis

## 4. Validation of the Numerical Approach

In this section, the proposed numerical approach is validated through an experimental test with a small scale CT specimen. Since the accuracy of the simulated response of the SEC sensor is highly related to the accuracy of the size of the simulated crack, i.e. crack length and crack width, a two-stage validation is necessary. It includes 1) validation of the crack growth simulation method presented in Section 3.2 by verifying the capability of the FE model to predict the crack growth in the tested CT specimen; 2) validation of the capacitance calculation method presented in Section 3.3 using the experimentally measured capacitance. In what follows, the FE analysis is first introduced, followed by the presentation of the two-stage validation.

An FE model of the CT specimen is created in Abaqus 6.13. The geometric dimensions of the FE model are the same as the test specimen, as shown in Figure 2(a). To simulate crack growth, material properties of A36 steel considering damage evolution theory are defined in Table 1. Physical meanings of some material properties are illustrated in Figure 6(a). The yield stress and maximum tensile stress of the material are determined by uniaxial tensile test of a coupon specimen.

Table 1. Definition of material properties in the FE model

| Material property | Value |
|---|---|
| Young's modulus | $2.0\times10^5$ N/mm$^2$ |
| Poisson's ratio | 0.26 |
| Yield stress | 414 N/mm$^2$ |
| Stress at initial damage point (max tensile stress) | 552 N/mm$^2$ |
| Strain at initial damage point | 20% |
| Stress at failure point | 0 N/mm$^2$ |
| Strain at failure point | 35% |

Two types of shell elements are employed for the model including four-node (S4R) and three-node (S3) elements. Figure 8 shows the mesh distribution of the FE model, where a denser mesh is

adopted along the crack path. The smallest element is at the tip of the notch (Figure 8a) with a size of 0.25 mm × 0.25 mm, while elements at the corners have the largest size (7.9 mm). The model contains a total of 4095 elements. To generate fatigue crack, a cyclic load with a constant load range from 2.89 kN to 28.9 kN is applied to the FE model through the interior edges of both holes. The Abaqus/Standard module is selected as the solver for this analysis with variable step length.

Figure 8(b) shows a crack generated during the simulation, in which a series of elements are identified as failure elements and then removed automatically. Figure 8(c) shows the plastic strain at the tip of the crack. These results indicate that the crack growth is successfully simulated using the element deletion method.

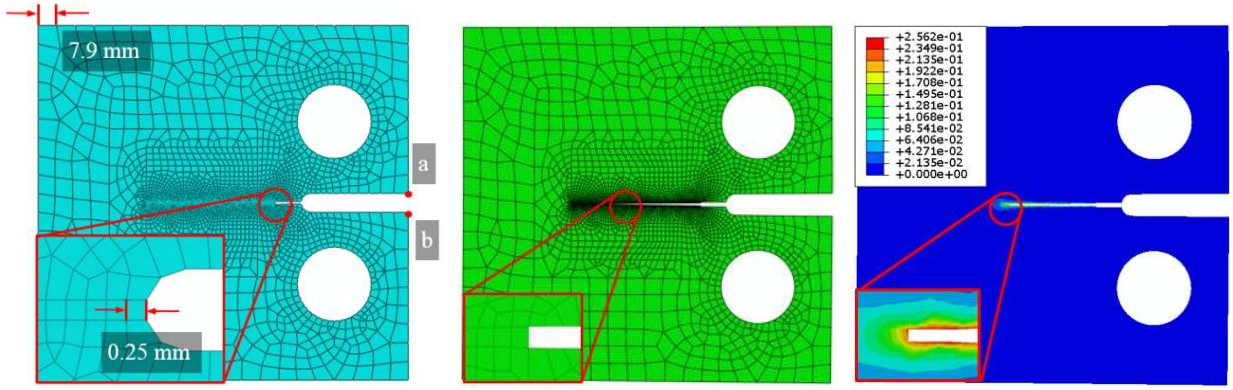


(a) (b) (c)

Figure 8. (a) Mesh distribution and typical element sizes; (b) simulation of crack growth; and (c) plastic strain at the crack tip

### 4. 1 Stage 1 validation: accuracy of simulated crack

The purpose of this validation is to verify the capability of the FE model to predict crack size in the tested specimen. This validation procedure is conducted by comparing the compliance at the front face of the CT specimen when the crack reaches certain lengths. Figure 9(a) shows the experimental setup, where a clip-on displacement gage (Epsilon model 3541) is mounted at the front face of the CT specimen through two knife edges to monitor the crack opening. Meanwhile, displacements at two points *a*, *b* at the same location in the FE model (Figure 8(a)) are collected for computing the crack opening. The compliance [29] at the front face of the CT specimen is defined as the ratio between the increment of crack opening $\Delta U$ measured by the clip gage and the increment of the applied load $\Delta F$ applied on the specimen (Figure 9(a)). Figure 9(b) shows a comparison of the FE model and the experimental dataset in terms of crack length vs. compliance. The crack lengths are measured by the adhesive measuring tape, starting from the tip of the notch (Figure 9(a)). The comparison shows a close match between test and FE model, indicating that the FE model can accurately predict the size of crack during crack growth.

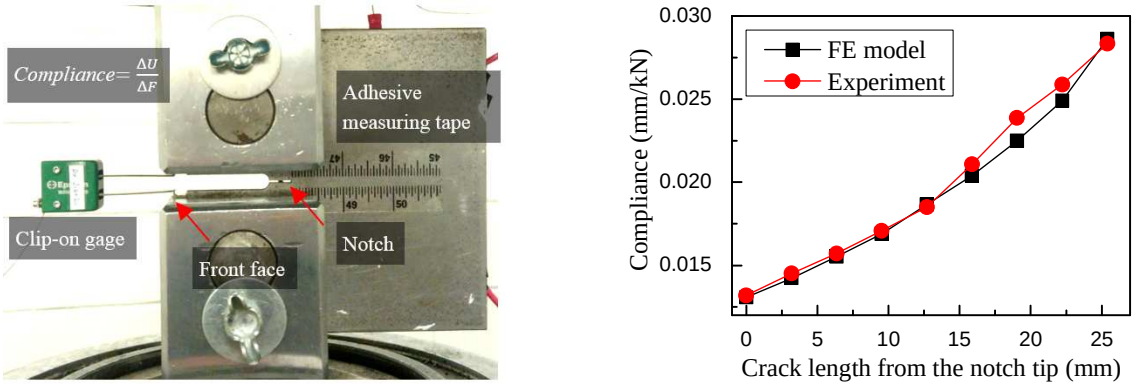


(a) (b)

Figure 9. (a) Installation of the clip-on displacement gage (the SEC sensor is attached to the back side of the specimen); and (b) compliance comparison between numerical and test results

## 4. 2 Stage 2 validation: accuracy of sensor's capacitance response

Once the mechanical behavior of the FE model has been validated, the simulated sensor's capacitance response can be evaluated. The experimental data presented in Section 2.2 is used for this validation.

As mentioned in Section 2.2, the peak-to-peak percentage change of capacitance ($PP\ C/C_0$) is selected as a measure for detecting crack growth. The reason is that the absolute capacitance of the SEC sensor is prone to drift due to environmental factors such as temperature and humidity change during long-term monitoring. Figure 10 shows the comparison between simulation results and raw experimental data when the crack grows for each 3.2 mm (1/8 in) increments in length. The crack length in these plots is taken as the distance measured between the tip of the crack and the edge of the sensing area (Figure 4). Comparison in Figure 10 shows substantial agreement between test data and simulation in both amplitude and phase. It demonstrates also that the crack growth can be monitored by the steady increment of $PP\ C/C_0$. For instance, a 0.1% capacitance change can be observed at 1.6 mm crack length, while the capacitance change increases by 3 times when the crack length reaches 17.5 mm.

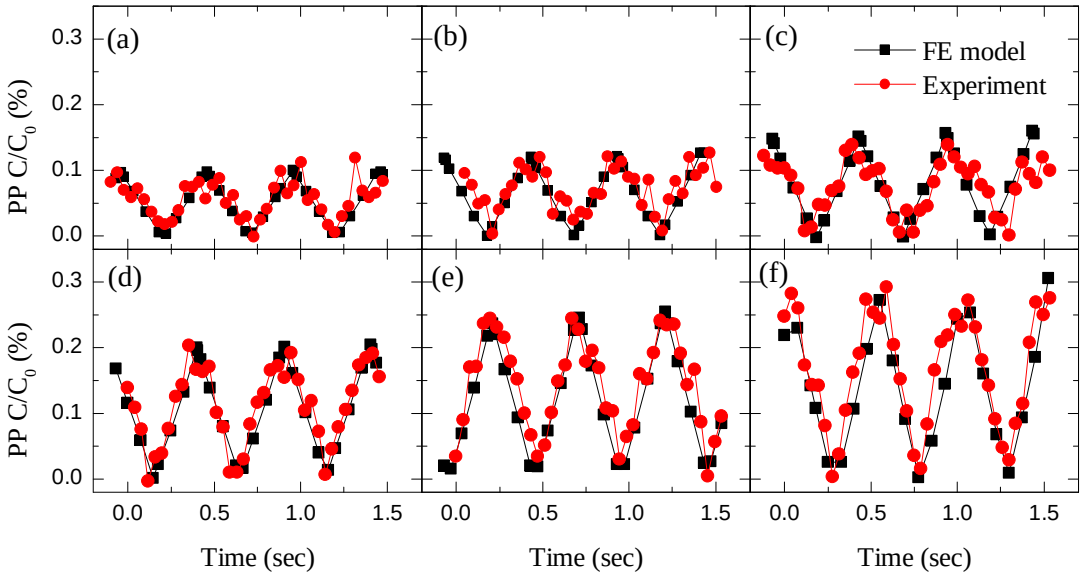


Figure 10. Comparison of the peak-to-peak percentage change of capacitance between simulation results and experimental data when the crack length reaches: (a) 1.6 mm; (b) 4.8 mm; (c) 7.9 mm; (d) 11.1 mm; (e) 14.3 mm; and (f) 17.5 mm

The comparison is further investigated in Figure 11 in terms of the *PP C/C₀* during the crack growth. The result indicates that the proposed numerical approach can predict a steady increment of capacitance change as the crack grows. This is in agreement with the experimental data also showing a similar trend, despite a smaller increment observable over short crack sizes (from 1.6 mm to 8.0 mm). This feature can be attributed to the noise content in the raw capacitance measurements, which challenges the identification of changes in the electrical signal under low strain.

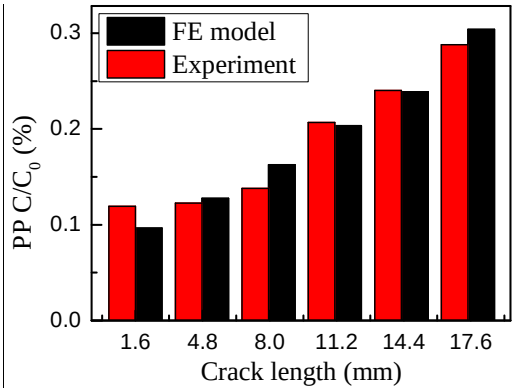


Figure 11. Comparison of the peak-to-peak percentage change of capacitance between simulation and experiment during the crack growth

Through the two-stage validation, the proposed methodology for numerical simulation has been verified for its ability to accurately predict sizes of the crack during propagation and the associated capacitance response of the SEC sensor. Following this validation, the methodology is applied to perform a parametric study to evaluate the effect of changing the size of the SEC sensor on its ability to detect fatigue cracks.

## 5 Crack monitoring with different sensor sizes

The SEC sensor can be fabricated or cut into different sizes to accommodate various application needs [17]. Sensors with larger size can monitor larger structural surfaces prone to cracking; however, the electrical sensitivity of the sensor ($\frac{\Delta C}{(\varepsilon_x+\varepsilon_y)} = \frac{C}{1-\nu}$) against crack growth decreases with increasing sensor size. In addition, the data acquisition (DAQ) system may be optimized for capacitance measurement when customized to a specific measurement range which is directly related to the sensor size. The motivation of this parametric study is to quantitatively evaluate the effect of the size of SEC sensors on the effectiveness of crack detection, and to provide guidance for dense sensor network optimization for practical applications.

Figure 12 shows four FE models of the CT specimen with different sizes of SEC sensor, which include 63.5 mm by 63.5 mm (full size), 47.6 mm by 47.6 mm (56% size), 31.8 mm by 31.8 mm (25% size), and 15.9 mm by 15.9 mm (6% size). Based on the geometric dimensions and material properties of the SEC sensor, the initial capacitance of the full size SEC sensor is 900 pF from Eq. (1), which is a typical value of the full size SEC sensor. Since the initial capacitance of the SEC sensor is proportional to the sensing area, initial capacitances of the 56% size, 25% size, and 6% size SEC sensors are computed as 506.3 pF, 225 pF, and 56.3 pF, respectively. The FE models are loaded with the same loading protocol described in Section 4. The capacitance responses of the SEC sensor are computed through the proposed algorithm.

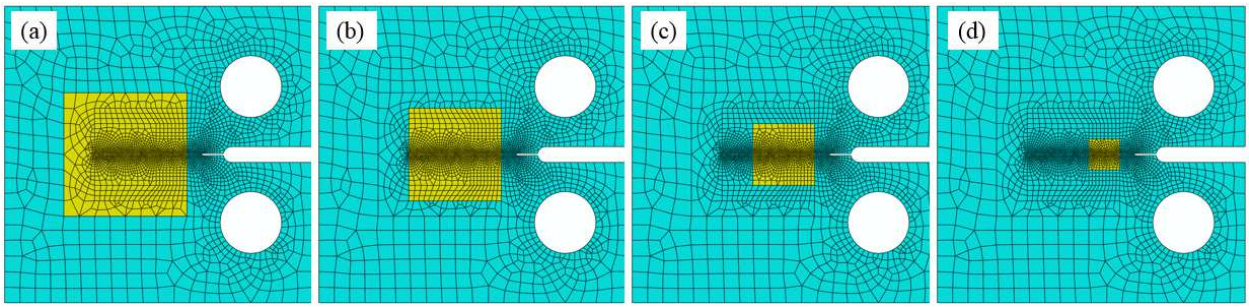


Figure 12. FE models with different sizes of sensing area, including (a) 63.5 mm by 63.5 mm (full size); (b) 47.6 mm by 47.6 mm (56% size); (c) 31.8 mm by 31.8 mm (25% size); and (d) 15.9 mm by 15.9 mm (6% size)

Results of this parametric study are shown in Figure 13. The crack length is measured as the distance between the tip of the crack and the edge of the sensing area (Figure 4). Both peak-to-peak percentage change (*PP C/C₀*) and peak-to-peak change of capacitance (*PP C*) are plotted in the figure against different sizes of the SEC sensor for three different crack lengths (1.6 mm, 7.9 mm, and 14.3 mm). Results indicate that both *PP C/C₀* and *PP C* increase as the crack grows in length. Take the 6% size SEC sensor as an example, as the crack grows from 1.6 mm to 14.3 mm, *PP C/C₀* increases from approximately 0.5% to 2.0%, and *PP C* increases from approximately 0.25 pF to 1.1 pF. Moreover, when the sensor size decreases, the peak-to-peak change in capacitance (*PP C*) decreases as well. However, the peak-to peak percentage change of capacitance (*PP C/C₀*) increases, indicating that a smaller SEC sensor is more sensitive to cracking. For instance, for the 14.4 mm crack, the sensitivity of the 6% size sensor is approximately 8 times higher than the full size sensor. The tradeoff is that it covers only 6% of structural surface

compared with the full size sensor. In practical applications, the optimal sensor size should be determined to achieve adequate sensitivity while maintaining as large coverage area as possible. A network may also be composed of several SECs of various size, depending on the required crack localization resolution. Figure 13 can also be used to predict the expected measurement range for detecting cracks under different lengths. The information can be used to optimize design of the DAQ system for capacitance measurement.

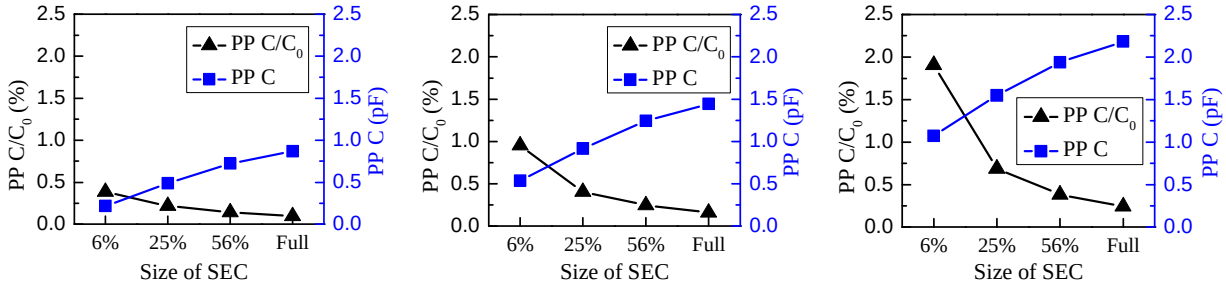


Figure 13. Capacitance change in terms of *PP C/C₀* and *ΔC* for different sizes of sensor when crack reaches different length: (a) 1.6 mm, (b) 7.9 mm, and (c) 14.3 mm

## 6 CONCLUSIONS

This paper furthers the understanding of a novel measurement method developed for detecting, localizing, and quantifying damage over mesosurfaces. This technology, the soft elastomeric capacitor (SEC), is a highly scalable strain gauge designed to be deployed in dense sensor network configurations to mimic biological sensing skin. The contribution of this paper is the development of a numerical approach to predict the SEC sensor's response under fatigue cracks.

The proposed approach consists of two parts: 1) simulating crack growth in the structure with FE analysis using an element deletion method, and 2) converting the FE analysis result into capacitance change of the SEC sensor. The numerical approach is validated by experimental data from a small scale CT specimen. The validation demonstrated that the numerical model of the CT specimen predicts accurate crack sizes during its propagation, and the proposed algorithm computes accurate capacitance response of the SEC sensor based on the FE result. The validated method is then applied to investigate the effect of changing the size of the SEC sensor on its ability to detect fatigue cracks. For the same crack size, smaller sensors are less sensitive in terms of peak-to-peak capacitance change, but more sensitive in terms of peak-to-peak percentage capacitance change. However, the coverage area may be greatly reduced by using a smaller sensor. The size of sensor therefore needs to be optimized to cover strategic areas at the desired resolution. The proposed approach enables dense sensor network applications of the SEC by linking the sensor's signal to a fatigue crack location and size. Being able to map a signal to engineering metrics is particularly helpful to infrastructure operators and managers by empowering them with the capacity to conduct condition-based maintenance.

## ACKNOWLEDGEMENT

This work was supported by the Transportation Pooled Fund Study, TPF-5(328), which includes the following participating state DOTs: Kansas, Iowa, Minnesota, North Carolina, Pennsylvania,

Texas, and Oklahoma, and Iowa Department of Transportation grant #RT454-494. Their support is gratefully acknowledged.

## REFERENCES

[1] Fisher JW 1984 *Fatigue and Fracture in Steel Bridges. Case studies* (Hoboken, NJ: Wiley-Interscience)

[2] Zhao Z, and Haldar A 1996 Bridge fatigue damage evaluation and updating using non-destructive inspections *Engineering fracture mechanics*. **53** 775-88

[3] Ihn JB, and Chang FK 2004 Detection and monitoring of hidden fatigue crack growth using a built-in piezoelectric sensor/actuator network: I. Diagnostics *Smart materials and structures*. **13**: 609

[4] Yu J, Ziehl P, Zárate B, and Caicedo J 2011 Prediction of fatigue crack growth in steel bridge components using acoustic emission *Journal of Constructional Steel Research*. **67** 1254-60

[5] Yeum CM, and Dyke SJ 2015 Vision‐Based Automated Crack Detection for Bridge Inspection *Computer-Aided Civil and Infrastructure Engineering*. **30** 759-70

[6] Adhikari RS, Moselhi O, and Bagchi A 2014 Image-based retrieval of concrete crack properties for bridge inspection *Automation in construction*. **39** 180-94

[7] Yao Y, Tung ST, and Glisic B 2014 Crack detection and characterization techniques—An overview *Structural Control and Health Monitoring*. **21** 1387-413

[8] Tikka J, Hedman R, and Silijander A 2003 Strain gauge capabilities in crack detection *4th International Workshop on Structural Health Monitoring.* 15-17

[9] Glisic B, and Inaudi D 2011 Development of method for in-service crack detection based on distributed fiber optic sensors *Structural Health Monitoring.* 1475921711414233.

[10] Loh KJ, Lynch JP, Shim BS, and Kotov NA 2008 Tailoring piezoresistive sensitivity of multilayer carbon nanotube composite strain sensors *Journal of Intelligent Material Systems and Structures.* **19** 747-64

[11] Dai H, Thostenson ET, and Schumacher T 2015 Processing and Characterization of a Novel Distributed Strain Sensor Using Carbon Nanotube-Based Nonwoven Composites *Sensors*. **15** 17728-47

[12] Yao Y, and Glisic B 2015 Detection of steel fatigue cracks with strain sensing sheets based on large area electronics *Sensors*. **15** 8088-108

[13] Loh KJ, Kim J, Lynch JP, Kam NW, and Kotov NA 2007 Multifunctional layer-by-layer carbon nanotube–polyelectrolyte thin films for strain and corrosion sensing *Smart Materials and Structures*. **16** 429.

[14] Mohammad I, and Huang H 2010 Monitoring fatigue crack growth and opening using antenna sensors *Smart Materials and Structures*. **19** 055023

[15] Yi X, Cho C, Cooper J, Wang Y, Tentzeris MM, and Leon RT 2013 Passive wireless antenna sensor for strain and crack sensing - electromagnetic modeling, simulation, and testing *Smart Materials and Structures*. **22** 085009

[16] Laflamme S, Ubertini F, Saleem H, D'Alessandro A, Downey A, Ceylan H, and Materazzi AL 2014 Dynamic characterization of a soft elastomeric capacitor for structural health monitoring *Journal of Structural Engineering*. **141** 04014186

[17] Laflamme S, Kollosche M, Connor JJ, and Kofod G 2012 Robust flexible capacitive surface sensor for structural health monitoring applications *Journal of Engineering Mechanics*. **139** 879-85.

[18] Laflamme S, Saleem HS, Vasan BK, Geiger RL, Chen D, Kessler MR, and Rajan K 2013 Soft elastomeric capacitor network for strain sensing over large surfaces *IEEE/ASME Transactions on Mechatronics*. **18** 1647-54

[19] Saleem H, Downey A, Laflamme S, Kollosche M, and Ubertini F 2015 Investigation of Dynamic Properties of a Novel Capacitive-based Sensing Skin for Nondestructive Testing *Materials Evaluation*. **73** 1384-91

[20] Kharroub S, Laflamme S, Song C, Qiao D, Phares B, and Li J 2015 Smart sensing skin for detection and localization of fatigue cracks *Smart Materials and Structures*. **24** 065004

[21] Kong X, Li J, Laflamme S, and Bennett C 2015 Fatigue Crack Monitoring using Large-area, Flexible Capacitive Strain Sensors. *The 6th International Conference on Advances in Experimental Structural Engineering (6AESE) and 11th International Workshop on Advanced Smart Materials and Smart Structures Technology (11ANCRiSST).* University of Illinois at Urbana-Champaign

[22] Kong X, Li J, Bennett C, Collins W, and Laflamme S 2016 Model calibration for a soft elastomeric capacitor sensor considering slippage under fatigue cracks. *SPIE Smart Structures and Materials + Nondestructive Evaluation and Health Monitoring* International Society for Optics and Photonics pp.98032P

[23] Simulia DS 2013 ABAQUS 6.13 User's Manual *Dassault Systems* Providence RI

[24] Song JH, Wang H, Belytschko T 2008 A comparative study on finite element methods for dynamic fracture *Computational Mechanics*. **42** 239-50

[25] Simonsen BC, Törnqvist R 2004 Experimental and numerical modelling of ductile crack propagation in large-scale shell structures *Marine Structures*. 17 1-27

[26] Movahhedy M, Gadala MS, Altintas Y 2000 Simulation of the orthogonal metal cutting process using an arbitrary Lagrangian–Eulerian finite-element method *Journal of materials processing technology*. **103** 267-75

[27] Bao Y, Kunnath SK, El-Tawil S, Lew HS 2008 Macromodel-based simulation of progressive collapse: RC frame structures *Journal of Structural Engineering*. **134** 1079-91

[28] Kong X, Shi T, Cheng S 2014 A numerical simulation method for steel structure collapsing under rare earthquake base on the material damage and failure law *China Civil Engineering Journal*. **47** 38-44

[29] Saxena A, Hudak Jr SJ 1978 Review and extension of compliance information for common crack growth specimens *International Journal of Fracture*. **14** 453-68